Comparative Lipidomic Analysis of Mouse and Human Brain with Alzheimer Disease*[S]

Robin B. Chan[‡§], **Tiago G. Oliveira**[‡§¶‖], **Etty P. Cortes**[§], **Lawrence S. Honig**[§**], **Karen E. Duff**[‡§], **Scott A. Small**[§**], **Markus R. Wenk**[‡‡§§], **Guanghou Shui**[‡‡§§1], and **Gilbert Di Paolo**[‡§2]

From the Departments of ‡*Pathology and Cell Biology and* **Neurology,* §*Taub Institute for Research on Alzheimer's Disease and the Aging Brain, Columbia University Medical Center, New York, New York 10032, the* ¶*Life and Health Science Research Institute (ICVS), School of Health Sciences, the* ‖*Life and Health Science Research Institute/3B's (Biomaterials, Biodegradables and Biomimetics), Portuguese Government Associate Laboratory, University of Minho, 4710-057 Braga, Portugal, the* ‡‡*Department of Biochemistry, National University of Singapore, Singapore 117597, and the* §§*Department of Biological Sciences, National University of Singapore, Singapore 117543*

Background: Lipid dyshomeostasis has been linked to Alzheimer disease (AD).
Results: Lipidomic analyses of brain tissue from AD patients reveal region-specific changes in multiple bioactive lipids, some of which are phenocopied in AD mouse models.
Conclusion: Lipid anomalies observed in AD may be linked to pathogenesis, including endolysosomal dysfunction.
Significance: This study highlights the hypothesis-generating potential of lipidomics and its applicability to other diseases.

Lipids are key regulators of brain function and have been increasingly implicated in neurodegenerative disorders including Alzheimer disease (AD). Here, a systems-based approach was employed to determine the lipidome of brain tissues affected by AD. Specifically, we used liquid chromatography-mass spectrometry to profile extracts from the prefrontal cortex, entorhinal cortex, and cerebellum of late-onset AD (LOAD) patients, as well as the forebrain of three transgenic familial AD (FAD) mouse models. Although the cerebellum lacked major alterations in lipid composition, we found an elevation of a signaling pool of diacylglycerol as well as sphingolipids in the prefrontal cortex of AD patients. Furthermore, the diseased entorhinal cortex showed specific enrichment of lysobisphosphatidic acid, sphingomyelin, the ganglioside GM3, and cholesterol esters, all of which suggest common pathogenic mechanisms associated with endolysosomal storage disorders. Importantly, a significant increase in cholesterol esters and GM3 was recapitulated in the transgenic FAD models, suggesting that these mice are relevant tools to study aberrant lipid metabolism of endolysosomal dysfunction associated with AD. Finally, genetic ablation of phospholipase D₂, which rescues the synaptic and behavioral deficits of an FAD mouse model, fully normalizes GM3 levels. These data thus unmask a cross-talk between the metabolism of phosphatidic acid, the product of phospholipase D₂, and gangliosides, and point to a central role of ganglioside anomalies in AD pathogenesis. Overall, our study highlights the hypothesis generating potential of lipidomics and identifies novel region-specific lipid anomalies potentially linked to AD pathogenesis.

Alzheimer disease (AD)[3] is a debilitating neurodegenerative disorder that afflicts millions of adults worldwide and the main cause of late life dementia. Three outstanding neuropathological features were noted in the original analysis from Alois Alzheimer, namely senile plaques, neurofibrillary tangles, and lipid granule accumulation (1). Based on the available molecular and biochemical techniques of the ensuing years, plaques and neurofibrillary tangles were viewed as consistent features of the AD brain and thus more heavily studied than changes in brain lipid metabolism (1). It is now common knowledge that the major molecular component of senile plaques is aggregated amyloid-β (Aβ), which is generated from the amyloid precursor protein (APP) via the sequential cleavage of APP by β-secretase β-site APP cleavage enzyme 1 (BACE1) and the γ-secretase complex, which contains a catalytic component, presenilin 1 or 2 (PS1 or 2). Although rare autosomal dominant mutations in APP and PS1 or 2 lead to early-onset familial AD (FAD) (2), the majority of AD cases are classified as late onset AD (LOAD). A major risk factor for LOAD is the E4 allelic variant of ApoE,

[3] The abbreviations used are: AD, Alzheimer disease; APP, amyloid precursor protein; BACE1, β-secretase β-site APP cleavage enzyme 1; PLD₂, phospholipase D₂; FAD, familial AD; PS1 and PS2, presenilin 1 and 2; LOAD, late onset AD; SM, sphingomyelin; pPE, plasmalogen phosphatidylethanolamine; PLC, phospholipase C; PA, phosphatidic acid; PFC, prefrontal cortex; ERC, entorhinal cortex; CRB, cerebellum; DAG, diacylglycerol; TAG, triacylglycerol; CE, cholesterol ester; PI, phosphatidylinositol; PC, phosphatidylcholine; PE, phosphatidylethanolamine; PS, phosphatidylserine; PG, phosphatidylglycerol; LBPA, lysobisphosphatidic acid; LPC, lysophosphatidylcholine; LPCe, lyso ether PC; Sulf, sulfatide; PI(4,5)P₂, phosphatidylinositol 4,5-bisphosphate; GM1, ceramide-N-tetrose-N-acetylneuraminic acid; GM3, ceramide-lactose-N-acetylneuraminic acid.

which encodes a protein involved in cholesterol metabolism and lipid transport (3). Importantly, a variety of genes have been recently linked to LOAD through genomewide association studies and are directly or indirectly connected to lipid metabolism or cellular membrane dynamics (4, 5).

Strong evidence now links AD with aberrant lipid homeostasis, in part for the following reasons (6, 7). First, neuronal lipid composition regulates the trafficking and/or activity of the key membrane-bound proteins controlling Aβ levels, including APP, BACE1, and presenilins. For instance, γ-secretase activity is regulated by membrane levels of cholesterol and sphingomyelin (SM) (8). Second, Aβ exerts its cytotoxic effects primarily by perturbing cellular membranes, in part by modulating the activity of phospholipases, such as PLA$_2$ (9), PLC (10), and phospholipase D$_2$ (PLD$_2$) (11). Third, lipids, such as ganglioside GM1, modulate the pathogenic potential of Aβ by affecting its propensity to aggregate (12). It is thus clear that an in-depth analysis of brain lipid composition changes in AD would provide a basis for further investigation of cell signaling and metabolic pathways that are disrupted in AD. Advances in lipidomics, particularly electrospray ionization-mass spectrometry, have facilitated the precise profiling of lipid species within tissues, including low abundance lipid classes that participate in cell signaling and membrane trafficking (13). Several studies focusing on defined families of lipids have made use of this technology to analyze lipid composition from AD brain tissue, showing changes in plasmalogen phosphatidylethanolamine (pPE) (14), sulfatide (Sulf) (15), ceramide (Cer), galactosylceramide (GalCer), cholesterol (16), and alkylacylglycerophosphocholine (17). Our own study has shown that a specific molecular species of phosphatidic acid (PA) previously linked to neurodegeneration in the fly (18) accumulates in the forebrain of old Swedish APP (swAPP) mice (11).

In this study, we present the lipidomic analysis of postmortem brain tissue obtained from patients with LOAD, specifically regions that typically are either moderately (prefrontal cortex, PFC) or severely (entorhinal cortex, ERC) affected in AD as well as a control region (cerebellum, CRB) that is largely unaffected by this disorder (19, 20). We also provide the lipidome of forebrain tissue obtained from three commonly used transgenic mouse models of FAD, namely (i) PSEN1$_{M146V}$ (PS1) (21), (ii) the Swedish mutant of APP$_{K670N,M671L}$ (APP) (22), and (iii) PS1-APP double transgenic (23) lines. Using a combination of normal phase and reverse phase LC-MS approaches, we analyzed 26 different lipid subclasses including lysophospholipids, glycerophospholipids, sphingolipids, glycerolipids, and sterols, covering over 300 lipid species. Our data show that multiple lipid subclasses are dysregulated in both the human AD tissue and AD mouse models, uncovering novel lipid pathways that may be linked to abnormal cellular activity and thus potential targets for further studies.

EXPERIMENTAL PROCEDURES

Annotation of Lipid Species—Glycerophospholipids, lysophospholipids, and diacylglycerol (DAG) were annotated as <lipid subclass> <total fatty acyl chain length>:<total number of unsaturated bonds>. Sphingolipids were annotated as <lipid subclass> <sphingoid base residue>/<fatty acyl res-

idue>. Triacylglycerol (TAG) was annotated as <TAG> <total fatty acyl chain length>:<total number of unsaturated bonds>/<fatty acyl residue>). Cholesterol ester (CE) was annotated <CE> − <fatty acyl residue>.

Human Brain Tissue—Frozen postmortem brain tissue samples were obtained from the New York Brain Bank at Columbia University Medical Center. Three different brain regions were sampled from different subjects: PFC, ERC, and CRB. Morphologically, each dissected region consisted predominantly of gray matter with minimal associated underlying white matter. AD was defined as "high probability of AD" based on NIA, National Institutes of Health-Reagan Institute (NIA-RI) criteria. Controls were free of major neuropathological diagnoses, and either did "not meet" or met "low probability of AD" by NIA-RI criteria. Further sample information, including a semiquantitative assessment of neuronal loss, neurofibrillary tangles, amyloid neuritic plaques, and Lewy body burdens, for the PFC and ERC, is presented in supplemental Dataset S3. On average, the ERC exhibited higher levels of pathology than the PFC in LOAD samples.

AD Mouse Models—A mixed population of wild-type, PS1, APP, and PS1-APP mice were described previously (21–24), aged between 9 and 11.5 months, were used for full lipidomics analysis in this study. An older group of wild-type and APP mice aged between 14 and 15 months were used for targeted PA analysis. SwAPP mice with the $Pld2^{+/+}$ and $Pld2^{-/-}$ genotypes with an average age of 12 months were described before (11) and used to examine the changes in sphingolipids and cholesterol ester. All mice were sacrificed by cervical dislocation, the forebrain dissected immediately and frozen in liquid nitrogen before storage at −80 °C.

Analysis of Lipids Using High Performance Liquid Chromatography-Mass Spectrometry—Lipid extracts were prepared using a modified Bligh/Dyer extraction procedure, spiked with appropriate internal standards, and analyzed using an Agilent 1200 HPLC system coupled with an Applied Biosystem Triple Quadrupole/Ion Trap mass spectrometer (3200Qtrap). Further cross-lab validation of our approach can be found in our previous work (25). Separation of individual lipid classes of polar lipids by normal phase HPLC was carried out using a Phenomenex Luna 3μ silica column (inner diameter 150 × 2.0 mm) with the following conditions: mobile phase A (chloroform:methanol:ammonium hydroxide, 89.5:10:0.5), B (chloroform:methanol:ammonium hydroxide:water, 55:39:0.5:5.5); flow rate of 300 μl/min; 5% B for 3 min, then linearly changed to 30% B over 24 min and maintained for 5 min, and then linearly changed to 70% B over 5 min and maintained for 7 min. Then, the gradient was changed back to the original ratio over 5 min and maintained for 6 min for column re-equilibration. Multiple reaction monitoring transitions were set up for quantitative analysis of various polar lipids (26, 27). Individual lipid species were quantified by referencing to spiked internal standards. PC, 14:0/14:0; PE, 14:0/14:0; PS, 14:0/14:0; PA, 17:0/17:0; PG, 14:0/14:0; d_{31}-PI, 18:1/16:0; C8-GluCer, C17-Cer, C12-Sulfatide, and C12-SM were obtained from Avanti Polar Lipids (Alabaster, AL). Dioctanoyl phosphatidylinositol (PI, 16:0-PI) was used for lysophosphatidylinositol quantitation and obtained from Echelon Biosciences, Inc. (Salt Lake City, UT).

TABLE 1
Average age at time of death, cold, and frozen postmortem intervals of patients used in this study

	Prefrontal cortex		Entorhinal cortex		Cerebellum	
	Control	AD	Control	AD	Control	AD
Number of samples	10	10	8	10	10	10
Age (yrs)	78.7 ± 8.2	83.2 ± 5.3	82.0 ± 5.2	85.4 + 5.2	85.0 ± 5.4	85.4 + 3.3
Cold PMI (h)	6.4 ± 4.6	6.4 ± 7.5	4.5 ± 4.9	4.8 ± 8.1	2.3 ± 1.0	4.1 ± 6.4
Frozen PMI (h)	15.0 ± 15.1	19.2 ± 11.0	20.3 ± 7.8	18.2 ± 8.2	18.8 ± 8.2	16.3 ± 6.5

TAG, DAG, and CE were analyzed using a modified version of reverse phase HPLC-electrospray ionization-MS described previously (28). Briefly, separation of TAG and CE from polar lipids was carried out on an Agilent Zorbax Eclipse XDB-C18 column (inner diameter 4.6 × 150 mm) using an isocratic mobile phase chloroform, methanol, 0.1 M ammonium acetate (100:100:4) at a flow rate of 250 μl/min. TAG were calculated as relative contents to the spiked d_5-TAG 48:0 internal standard (CDN isotopes), whereas cholesterol esters were normalized to corresponding d_6-C18 cholesterol ester (CDN isotopes). DAG species were quantified using 4-methyl 16:0 diether DAG as an internal standard (Avanti Polar Lipids). Free cholesterol was analyzed by reverse phase HPLC atmospheric pressure chemical ionization MS, utilizing the same XDB-C18 column as above but with chloroform:methanol, 1:1 (v/v), as the mobile phase at a flow rate of 500 μl/min (29). The instrument was operated in the positive mode with a vaporizer temperature of 500 °C and corona current of 3 μA. Free cholesterol was quantified relative to spiked d_6-cholesterol (CDN isotopes) internal standard.

Data Analysis and Presentation—Lipid levels for each sample were calculated by summing up the total number of moles of all lipid species measured by all three LC-MS methodologies, and then normalizing that total to mol %. The final data are presented as mean mol % with error bars showing mean ± S.E. All lipid species in the human samples and more than 98% of the lipid species measured in the mouse samples were found to have equal variance (data not shown). For the human samples, a two-tailed Student's t test was used for statistical analysis. The mouse data were analyzed by one-way analysis of variance followed by post hoc multiple comparisons Tukey range test as indicated accordingly. In all cases, *, $p < 0.05$; **, $p < 0.01$; ***, $p < 0.001$. For all bar graphs, error bars represent the mean ± S.E.

RESULTS

Comparative Lipid Profiling of Postmortem Human Brain Tissue—Postmortem brain tissues obtained from both control and AD patients with similar average age, cold, and frozen postmortem intervals were used in our analysis (Table 1). Depending on brain region, ~44–48% of the lipidome measured in our analysis was made up of free cholesterol (Fig. 1, supplemental Fig. S1A and Dataset S1A). The next largest group is comprised of the glycerophospholipids, the bulk of which is made up of phosphatidylcholine (PC) (14.4–17.5%), phosphatidylethanolamine (PE) (4.0–6.3%), and pPE (8.0–9.8%). Other glycerophospholipids of intermediate abundance are phosphatidylserine (PS) (2.5–4.2%), phosphatidylinositol (PI) (2.4%-2.8%), and ether PC (ePC) (1.3%). Very low abundance glycerophospholipids were also measured including lysophospholipids (0.84–

1.12% total), PA (0.16–0.25%), phosphatidylglycerol (PG) (0.06–0.09%), and lyso-bisphosphatidic acid (LBPA) (0.013–0.025%). In addition, we also measured a wide array of sphingolipids such as SM (7.7–9.5%), Cer (1.0–1.3%), glucosylceramide (GluCer) (1.4–2.6%), GalCer (1.4–2.4%), ganglioside GM3 (0.050–0.083%), and Sulf (1.1–2.1%). Comparatively, glycerolipids such as DAG (0.33–0.62%) and TAG (0.05–0.10%) and sterol derivative CE (0.31–0.62%) make up a very small proportion of the entire lipidome. The detailed molecular distribution of the individual lipid species measured can be found in supplemental Figs. S2–S4 and Dataset S1B. The PFC and ERC had a similar fatty acyl chain profile, consisting mostly of medium (36C) and long (>38C) chain fatty acyls and with either monounsaturated or polyunsaturated fatty acids with 4 or 6 bonds (Fig. 3, *A*, *B*, *D*, and *E*). Surprisingly, the CRB exhibited a unique fatty acyl profile, with the highest proportion from medium-chain length (36C) and monounsaturated phospholipids (supplemental Fig. S1, *B* and *C*). However, all three brain regions are highly similar in terms of sphingolipid chain length, with the majority being long (>42C) or medium (36C) chain length (Fig. 3, *C* and *F*, and supplemental Fig. S1D).

Postmortem AD Tissue Display Region-specific Differences in Lipid Metabolism—Overall, whereas the lipid profile of the CRB from AD patients was comparable with that of control subjects (supplemental Figs. S1 and S4), the lipid profiles of both PFC and ERC were affected by the disease (Fig. 1). In the PFC, the most striking change was observed for DAG, which showed an overall 1.8-fold increase in AD (Figs. 1A and 4, and supplemental Fig. S2 and Dataset S1). Although numerous species of DAG were up-regulated, a pool of DAG (38:4) believed to derive from the PLC-mediated cleavage of phosphatidylinositol 4,5-bisphosphate (PI(4,5)P$_2$) and thus involved in signaling (30), was up-regulated by ~2.1-fold (supplemental Fig. S2). Analysis of glycerophospholipids showed an overall decrease in the levels of lysophosphatidylcholine (LPC) and lyso ether PC (LPCe) (~19 and ~13%, respectively), but no changes in PC. There was a clear decrease in total PE (~25%), including major PE species, 40:6, 38:6, and 38:4. Contrary to a previous report (14), lower pPE levels were not seen except for a slight decrease in a single species, PE, 38:6p. Specific pools of ePC, 34:0p, 34:1p, and 32:1e, were up-regulated, whereas PC 34:0e was down-regulated. In the overall fatty acyl distribution, there was a decrease in long-chain fatty acids (>40C) with a corresponding increase in short-chain fatty acids (34C) (Fig. 3, *A* and *B*). Sphingolipid metabolism was also perturbed in AD samples, with a ~25% decrease in medium length species (Fig. 3C). Although medium length SM d18:0/20:0 and d18:1/20:0 were subtly down-regulated, long-chain species SM d18:1/22:1 and d18:1/26:1 were up-regulated. The overall Cer levels were increased by ~33%,
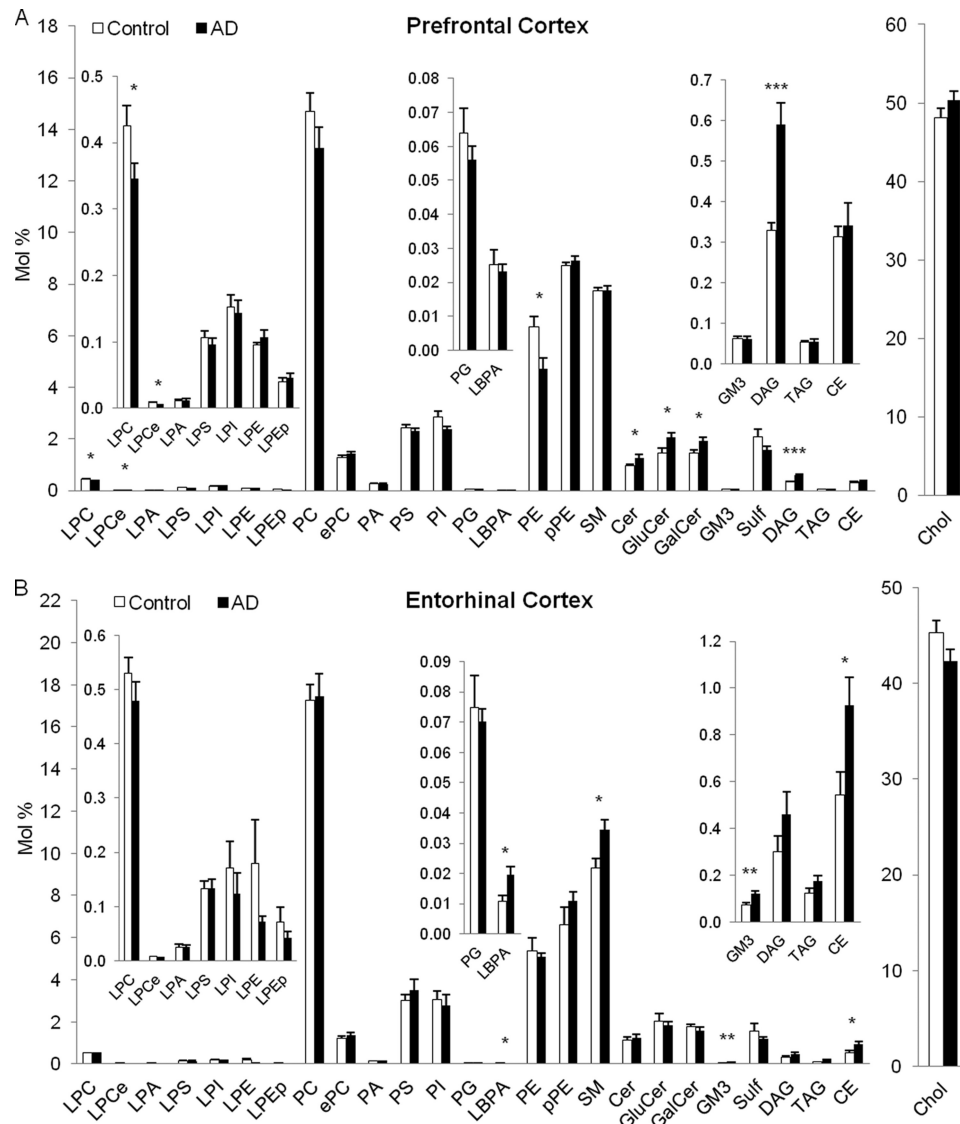
FIGURE 1. **Postmortem human brain tissue lipid composition is altered in LOAD.** Various lipid changes are seen in PFC (*A*) and ERC (*B*) tissues. Lipid subclasses are expressed as mean mol % of all lipid species measured with *error bars* indicating mean ± S.E. The sample size for each brain region analyzed is shown in Table 1. The absolute level of individual lipid species is presented in supplemental Dataset S1.

mostly due to the major Cer species d18:1/18:0. However, there was a clear metabolic shift toward an increase of simple glyco-sphingolipids GluCer (~43%) and GalCer (~32%), perhaps reflecting increased catabolism of Sulf (which were decreased by ~25%) (see also Ref. 15).

The ERC tissue exhibited a different pattern of lipid altera-tions compared with the PFC (Figs. 1*B* and 4, supplemental Fig. S3 and Dataset S1). LBPA (also called bis(monoacylglyceryl)-phosphate), a lipid that is synthesized primarily from PG and highly enriched in the endolysosomal system (31), was highly enriched in AD (~1.8-fold), including numerous species such as 32:1, 34:3, 36:3, 36:1, and 38:5 (supplemental Fig. S3). This region also showed increased levels in multiple species of the polyunsaturated lipid pools including PC 38:4p, 40:5p, and PE 36:5, 38:5, and 36:3p. Unlike the PFC, AD-affected ERC also exhibited alterations in different subclasses of sphingolipids, specifically increases in SM and ganglioside GM3 (~20 and ~64%, respectively). Strikingly, whereas SM species with a

shorter fatty acyl residue including d18:0/18:0, d18:1/16:1, and d18:1/18:0 were selectively enriched, GM3 enrichment was restricted mainly to those with longer chain fatty acyl residues such as d18:0/24:0, d18:1/22:0, and d18:1/24:0 (supplemental Fig. S3). The selective increase in higher abundance SM led to a modest boost in overall short-chain sphingolipids distribution (Fig. 3*F*). Last, levels of CE, *i.e.* lipids typically enriched in lipid droplets (31), were significantly higher in ERC with AD (~1.7-fold), particularly in the form of CE-16:1, CE-16:0, and CE-18:1. Interestingly, select pools of TAG (*e.g.* TAG 56:7(22:6) and 56:5(18:1)), which are also enriched in lipid droplets (32), accu-mulated in AD-affected ERC (supplemental Fig. S3).

Comparative Lipid Profiling of FAD Mouse Models Forebrain Brain Tissue—To determine whether any of the lipid changes seen in LOAD are phenocopied in the brain of commonly used mouse models of FAD, we characterized the forebrain lipid composition of WT, PS1, APP, and PS1-APP mice within an age range (*i.e.* 9–11.5 months) where transgenic mice have been
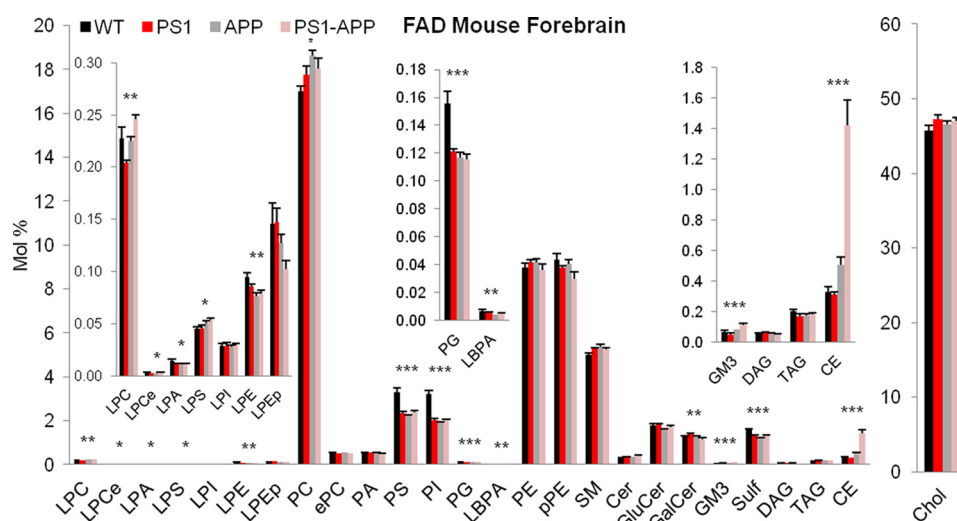
FIGURE 2. **Effects of FAD transgene expression on mouse forebrain lipid composition.** Aberrant lipid homeostasis is evident in different FAD mice. Lipid subclasses are expressed as mean mol % of all lipid species measured with *error bars* indicating mean ± S.E. (WT, $n = 6$; PS, $n = 6$; APP, $n = 6$; PS-APP, $n = 6$). Statistical significance shown here was assessed by one-way analysis of variance analysis. The absolute level of individual lipid species is presented in supplemental Dataset S2.

characterized for various biochemical, morphological, electrophysiological, and behavioral phenotypes. Although the PS1 mice exhibit subtly increased Aβ42 levels without noticeable pathology (21), the APP mice show significantly elevated Aβ levels and develop numerous plaques between 9 and 13 months (22). Comparatively, Aβ production is markedly increased in the PS1-APP mice, which begin developing a severe plaque burden by 6–7 months (23). Reflecting in part the severity of Aβ burden, synaptic and behavioral impairments are least apparent in the PS1 mice and highly exacerbated in the PS1-APP mice (23, 24).

The comprehensive lipid composition of the forebrain tissue of the different mice is shown in Fig. 2, supplemental Fig. S5 and Dataset S2. As with the case of the human AD tissue, free cholesterol levels occupied the bulk of the lipidome we measured. The remainder of the WT mouse forebrain lipidome is composed mainly of bulk glycerophospholipids such as PC (17.0%), PE (9.0%), pPE (9.3%), PS (3.3%), PI (3.2%), and to a lesser extent sphingolipids such as SM (5.0%), GluCer (1.8%), GalCer (1.3%), and Sulf (1.6%). Contributing about 2% of the lipidome are low abundance glycerophospholipids such as lysophospholipids (0.56% total), ePC (0.52%), PA (0.52%), PG (0.16%), LBPA (0.007%), sphingolipids including Cer (0.34%), and GM3 (0.069%), glycerolipids DAG (0.058%) and TAG (0.2%) and sterol derivative CE (0.33%). The majority of phospholipids found in the mouse forebrain carry long-chain fatty acyls composed of 38 or more total carbon lengths, whereas medium (36C) and short-chain (<34C) length fatty acyls are less abundant (Fig. 3G). Corresponding to the long fatty acyl chain length, the majority of the phospholipids are polyunsaturated with either 4 or 6 double bonds (Fig. 3H). Phospholipids with the monounsaturated bond are the third most abundant followed by fully saturated phospholipids. Similar to the human brain tissue profile, the majority of sphingolipid species are either long (>42C) or medium (36C) chain length (Fig. 3I).

Lipid Dysregulation in FAD Mouse Models—All three AD transgenic mouse models showed distinctive lipid profiles com-pared with the WT mice (Fig. 2, 4, supplemental Fig. S5 and Dataset S2). Fatty acyl chain remodeling was evident, with an overall decrease in long-chain phospholipid (C > 40), and a corresponding increase in medium- to short-chain phospholipids (C < 36) (Fig. 3G). Related to these changes, a decrease in fatty acyl chains carrying four polyunsaturated bonds was also replaced by an increase in monounsaturated and saturated fatty acyls (Fig. 3H). In the APP and PS1-APP mice but not the PS1 mice, there was a similar decrease in long-chain sphingolipids (C > 40) that was balanced by increases in short and medium length species (C = 36 to 38) (Fig. 3I).

In the PS1 mutants, there was a significant decrease in PS (~29%), PI (~37%), PG (~25%), and LBPA (~29%) as well as in LPC (~13%) and LPCe (~20%). Individual PA pools were also highly dysregulated, with PA 34:1 and 36:1 having increasing trends, whereas other species such as PA 32:1, 34:2, and 38:4 were decreased significantly (supplemental Fig. S5). Various pools of the most abundant sphingolipid SM, such as SM d18:1/18:0, and long-chain SM d18:1/26:1 and d18:0/24:0, were selectively enriched. Unique to the PS1 mutant was an increase in long-chain GalCer species such as GalCer d18:1/24:1, d18:1/24:0, and d18:1/26:0, which could be attributed to the degradation of Sulf (~17%) (supplemental Fig. S5). Contrary to an earlier study on PS1 mutant hippocampus (33), we found no increase in Cer.

Similar to the other transgenic mice, the APP mutant showed decreased levels of PS (~33%), PI (~41%), PG (~25%), LBPA (~43%), and LPE (~20%) with an overall increase in PC (~10%). A decrease in various molecular species of PA (*e.g.* 32:1 and 34:2) was also observed. These data are in contrast to the specific increase of PA 34:2 seen in a different strain of Swedish APP transgenic mice that were also older in age (11). To determine whether this was an age-related phenomenon, we conducted a targeted PA analysis of 14–15-month-old APP mice of the same genetic background and found that PA 34:2, and to a lower extent other molecular species of PA, were indeed elevated in these mice relative to 9–11-month-old APP mice
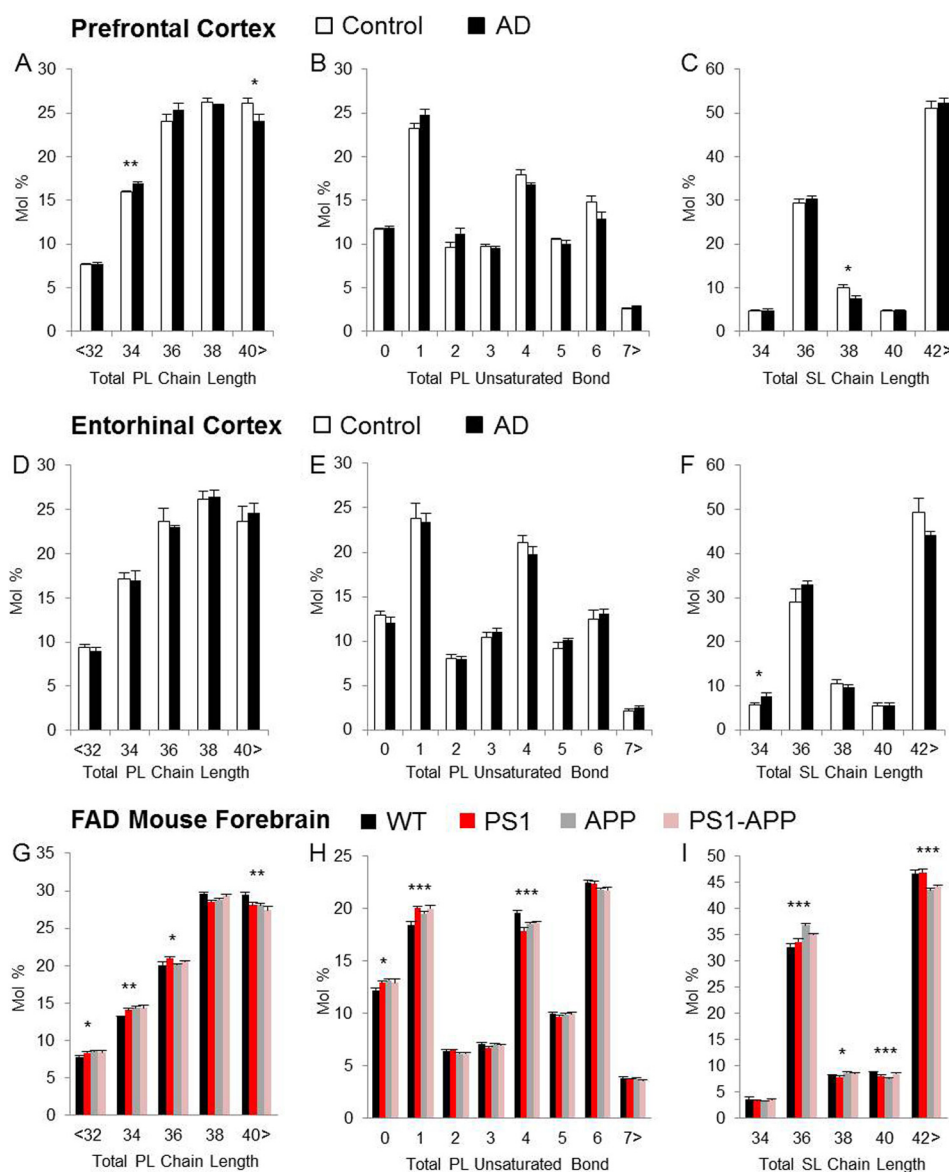
FIGURE 3. **Altered fatty acid composition of postmortem human brain tissue in the PFC and ERC regions and of forebrain derived from FAD mouse models.** Independent analyses for changes in diacylglycerophospholipids (*GP*) and DAG chain length equal to the total number of carbon atoms in the sum of fatty acid moieties (*A*, *D*, and *G*), GP and DAG saturation equal to the total number of double bonds in the sum of fatty acid moieties (*B*, *E*, and *H*), sphingolipid (*SL*) chain lengths equal to the total number of carbon atoms in both long-chain base and fatty acid moieties (*C*, *F*, and *I*) are expressed as mol %.

(supplemental Fig. S6). Similar to the PS1 mutant, an increase in SM was observed in APP mice, reflecting the selective accumulation of medium-chain length SM d18:1/18:1, d18:1/18:0, and d18:0/18:0. This may have resulted from either increased catabolism of GluCer and/or Sulf, both of which showed significant decreases (~10 and 26%, respectively). Finally, the APP mice showed a trend for increasing total levels of GM3 and CE as represented by specific molecular pools such as GM3 d18:1/18:0 and CE-22:6 (supplemental Fig. S5).

The PS1-APP mutant forebrain was the most severely affected, reflecting the additive or synergistic effects of the two transgenes. Similar to both the PS1 and APP mice, there was a major loss of lipids from the PS (~28%), PI (~37%), PG (~25%), and LBPA (~29%) subclasses and a slight increase in overall PC levels. Unlike the single transgenics, PS1-APP mice showed a decrease in pPE 34:2, 36:2, 36:1, and 36:0 as well as an increase

in lysophospholipids, such as lyso-PS (LPS) (~17%), lyso-PA (LPA) (~21%), and lyso-PE (LPE) (~16%). The changes in sphingolipid profile, specifically an increase in SM pools such as SM d18:1/18:0 and other long-chain species, and significant decrease in total Sulf (~17%), also resemble the changes of the other two mutants. However, two groups of lipid alterations were prominent in the PS1-APP mice. First, there was an enrichment of GM3 (~1.7-fold), particularly with major species GM3 d18:0/18:0, d18:1/18:0, and d18:1/20:0 (supplemental Fig. S5). Second, total CE levels was highly enriched (~4.3-fold), with a dramatic increase (~11-fold) for specific species, such as CE-22:6 (supplemental Fig. S5).

PLD$_2$ Ablation Causes Normalization of GM3 Levels—Lipidomics can be harnessed to identify lipid pathways that are specific to perturbations made to different biological systems (34, 35). Combining our current data set with pharmacological

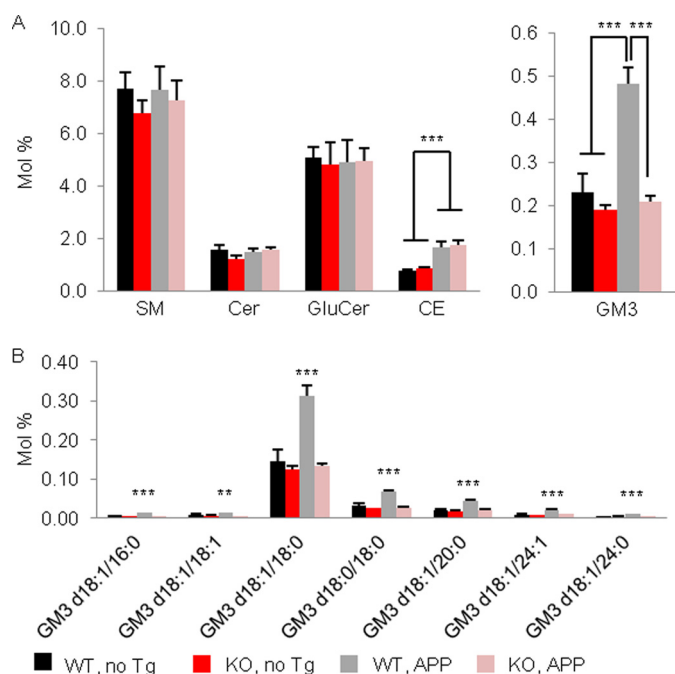## Lipid Profiling of Brain Tissue with Alzheimer Disease
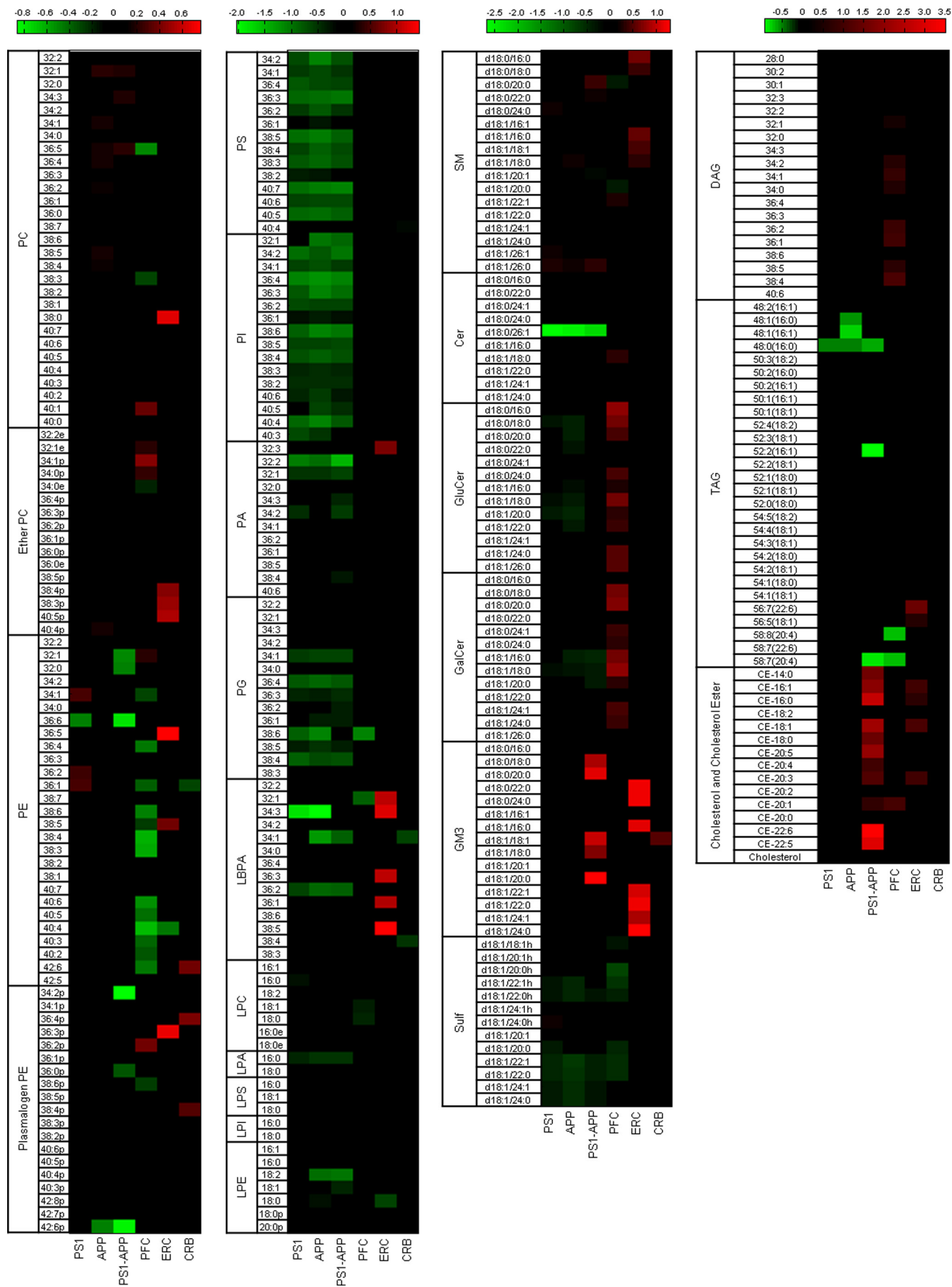
FIGURE 5. **PLD$_2$ ablation normalizes GM3 levels in an AD mouse model expressing Swedish APP transgene.** *A*, the overall sphingolipid and cholesterol ester levels, and *B*, individual GM3 species in the forebrain of these mouse models are presented as mean mol % with *error bars* indicating mean ± S.E. (*WT, no Tg*, $n = 8$; *KO, no Tg*, $n = 6$; *WT, APP*, $n = 5$; *KO, APP*, $n = 6$).

treatments or genetic models that affect pathophysiological phenotypes of AD may identify *bona fide* targets of the disease. We recently reported that swAPP transgenic mice lacking PLD$_2$, which hydrolyzes PC to generate PA, are protected from the synaptotoxic and memory-impairing actions of Aβ *in vitro* and *in vivo* (11). This protection occurs despite the production of high amounts of Aβ indicating that the toxic effects of Aβ may be neutralized. To understand the molecular basis of this protection, we conducted a targeted lipidomic analysis of the forebrain of these mice, which were slightly older than those used in Figs. 2–4 (see "Experimental Procedures"). Although most sphingolipid classes appear to be unaltered in the mutant mice, profound alterations were observed for GM3 and CE (Fig. 5A). In the *Pld2$^{-/-}$* only mice, most molecular species of GM3 were slightly reduced in the forebrain. In contrast, expression of the swAPP transgene alone produced a significant increase in GM3 and CE, similar to the PS1-APP animals (Fig. 2). Most importantly, when swAPP expression and PLD$_2$ ablation were combined, GM3 but not CE levels were normalized, suggesting that ganglioside metabolism may be correlated to the pathogenicity associated with the swAPP model and its rescue in the *Pld2$^{-/-}$* background (Fig. 5B).

DISCUSSION

In the present study, we conducted an in-depth lipidomic analysis of AD brain tissue that covered over 300 lipid species

from 26 lipid subclasses. We observed that different regions of the human brain undergo heterogeneous changes in lipid metabolism in AD-affected patients. Although the CRB lipid profile was largely unaffected, significant changes were observed in the diseased PFC and ERC (Fig. 1 and supplemental Fig. S1). Between these two tissues, the PFC seemed to carry more severe lipid alterations, with decreased levels of LPC, LPCe, and PE and elevated levels of Cer, GluCer, GalCer, and DAG. In contrast, the ERC only showed significant increases in LBPA, SM, GM3, and CE levels. However, there were also numerous changes to individual lipid species in different subclasses, suggesting that fatty acid carbon chain specificity may play an important role in AD pathogenesis (Fig. 4 and supplemental Figs. S2 and S3). In the PFC, this included various molecular species from the ePC, SM, Sulf, and CE, whereas ERC displayed variability in ePC, PE, and TAG. Importantly, the differences in lipid signatures suggest that these two subregions encounter different aspects or stages of AD pathogenesis, as supported by functional and pathological analyses (19, 20). As expected, neuronal loss was more obvious in the ERC than in the PFC (supplemental Dataset S3). Because neuronal loss is typically associated with gliosis, the lipidome of regions undergoing significant neuronal loss, such as the ERC, may reflect in part changes in the neuron/glia ratio.

Because mouse models are used extensively to study AD pathogenesis, we set out to define whether specific changes in lipid metabolism in brain tissue with LOAD are phenocopied by mouse models of FAD and if these pathways can be targeted for further studies. Granted, this type of comparative analysis faces inherent challenges, including species-specific differences and disease etiology (*i.e.* FAD *versus* LOAD), and are thus not expected to be a perfect model for studying LOAD. With these caveats in mind, we observed dramatic lipid changes in all three transgenics that were not seen in humans. Specifically, a variety of anionic phospholipids and sphingolipids, such as Sulf, were decreased in transgenic models. Furthermore, genotype-specific lipid changes were observed and in several cases, the alterations present in the PS1-APP mice reflected an additive or synergistic effect of bigenic FAD gene expression. For instance, PS1-APP mice exhibited a striking elevation of CE and GM3, which was present to a lower extent in the APP mice and virtually absent from PS1 mice (Fig. 2 and supplemental Fig. S5).

Our analysis points to dysregulation of specific lipids potentially involved in key anomalies seen in AD including synaptic dysfunction and neurotransmission deficits (36). For instance, DAG metabolism, which is highly aberrant in diseased PFC, has been implicated in a number of synaptic processes including the regulation of dendritic spine morphology, plasticity, and neurotransmitter release (37). Importantly, overactivation of PKC, a target of DAG, interferes with PFC-regulated working memory (38), a key feature of AD. DAG accumulation in

---

FIGURE 4. **Comparative lipid profile of LOAD human samples *versus* FAD transgene expressing mouse forebrains.** The heat maps show all lipid species measured and are organized according to phospholipids, sphingolipids, and neutral lipids classification. The *PS, APP*, and *PS1-APP* columns represent the normalized values of the individual lipid species of mutant mice compared with wild-type mice, whereas the *PFC, ERC*, and *CRB* columns represent the normalized values of the individual lipid species of LOAD patients compared with control patients for each tissue type. The *color bars* represent the log2 value of the ratio of each lipid species and only statistically significant changes are shown ($p < 0.05$). Statistical analysis for the mouse data is based on one-way analysis of variance and post hoc Tukey range test.

the PFC likely occurs through Aβ-stimulated hydrolysis of PI(4,5)P$_2$ by PLC (10), based on the specific accumulation of polyunsaturated DAG 38:4 (supplemental Fig. S2), a primary metabolite of PI(4,5)P$_2$ (30). Compounding this effect may be the loss of DAG kinase activity because synaptic targeting of DAG kinase depends on PSD95, whose levels are decreased in AD-affected brain tissue (11, 37). Furthermore, aberrant accumulation of sphingolipids in the PFC may also contribute to dysregulation of synaptic vesicle fusion and trafficking of NMDA receptors (39). This may reflect the fact that Aβ42 activates neutral sphingomyelinase, which produces Cer (8), and that sphingolipid enzymes are significantly altered in this tissue (40). Overall, our data suggest that aberrant DAG and sphingolipid metabolism are likely to participate in synaptic dysfunction in diseased PFC.

Another important observation is the LBPA increase in diseased ERC. LBPA is enriched specifically within late endosomes, where it plays a role in the biogenesis of multivesicular bodies (41). The enrichment of LBPA is thus consistent with a dysfunction of the late endosomes/multivesicular bodies. Aberrant endosomes have been previously reported in Down syndrome and AD (42) and growing evidence, most recently through genome wide association (4, 5) and gene expression (43) studies, indicates that defects in the endolysosomal pathway are linked to AD. An emerging hypothesis in the field is that defects in the endolysosomal pathway can affect amyloidogenesis, as organelles along this pathway contain high levels of APP as well as functionally active pools of BACE1 and γ-secretase (44, 45). Additionally, lysosomal defects alter the clearance of autophagosomes, which are double-membrane organelles of the autophagy pathway that mediate the elimination of protein aggregates, including Tau (45). Notwithstanding other possible functional implications (see below), the ERC accumulation of SM, GM3, and CE adds strong support to the endolysosomal dysfunction hypothesis. Indeed, SM and GM3 traffic within and between the plasma membrane and endosomes (46), whereas intracellular CE, normally found in lipid droplets, has also been detected in late endosomes (47). Of particular relevance, the accumulation of SM and gangliosides impairs lysosomal degradation of APP-CTFs, which enhances amyloidogenesis (48). A likely secondary implication of SM and GM3 accumulation is the propensity for ganglioside-enriched membrane microdomains at the cell surface and in endosomes to seed Aβ oligomerization (12). Taken together, the overall lipid profile changes seen in the ERC of AD patients suggest a pathogenic cascade that is reminiscent of lipid traffic jams described in lipid storage diseases such as Niemann-Pick types A and C (49).

Although lipid changes in FAD models are in most aspects vastly different from the LOAD samples, our lipidomic analysis suggest that the APP and PS1-APP mice are likely suitable models to study the role of ganglioside (GM3) and CE accumulation in AD, particularly because these anomalies are also observed in the ERC of AD patients (Fig. 4). A key question is whether the reversal of these lipid changes can ameliorate the AD-relevant phenotypes of the transgenic models, including enhanced amyloidogenesis. A partial answer, as well as an important "proof of concept" validation of our analysis, is that the pharmacological inhibition and genetic ablation of acyl-coenzyme A:cholesterol

acyltransferase 1, a CE-synthesizing enzyme, lower Aβ production and improves memory related tasks in transgenic models of AD (32). Our own studies suggest that the protective role of PLD$_2$ ablation in APP transgenic mice may be related to gangliosides, as suggested by the normalization of GM3 levels to those found in control mice (Fig. 5). This raises important questions about how PLD and its product PA are related to ganglioside metabolism and perhaps endolysosomal dysregulation in AD (11, 50). Additionally, because PLD$_2$ ablation mitigates the signaling, but not the biogenesis of Aβ (11), we hypothesize that the GM3 elevation observed in the APP models (which is corrected in the *Pld2* knock-out) occurs downstream of Aβ. Interestingly, the normalization of GM3 levels in the FAD mouse lacking PLD$_2$ occurs independently of CE, suggesting that CE elevation in FAD mice may not be driven by increased Aβ signaling *per se*. Overall, our data suggest that there are multiple ways to relieve lipid traffic jams that may be detrimental to neural cells in AD pathogenesis.

Finally, our study suggests that AD is associated with a more general perturbation of membrane properties. The length and degree of saturation are important determinants of many membrane characteristics including membrane thickness, fluidity, local curvature, and molecular packing, which in turn regulate the activities of membrane-bound enzymes (51). Intramembrane proteolysis is likely to be exquisitely regulated by membrane thickness, with major implications for γ-secretase-mediated cleavage of APP (52). Interestingly, FAD mouse forebrains and to a lower extent diseased PFC and ERC, exhibited a relative increase in short-chain lipids that was accompanied by a reduction in polyunsaturated phospholipids (Fig. 3). Similar results have been described in synaptosomal and detergent-resistant membranes due to aging (53) and AD (54). It is well known that long-chain polyunsaturated phospholipids display an aversion to highly ordered lamellar microdomains, whereas short-chain monounsaturated or saturated phospholipids interact favorably with sphingolipids and cholesterol in lipid rafts (6, 55). These features thus point to an increased propensity of membranes from the AD-affected brain to form lipid rafts, which may have consequences on the amyloidogenic processing of APP (6, 7).

A fundamental challenge in understanding a complex disease using a systems based approach, such as lipidomics, is the identification of pathophysiologically relevant changes among a myriad of changes. Here, we have capitalized on the exquisite sensitivity of LC-MS to characterize the lipidome of brain tissue from AD-affected humans and commonly used FAD mouse models. We describe novel region-specific lipid changes in human AD tissue that may contribute to AD etiology. We also identified overlaps in lipid dysregulation between mice and humans, suggesting that the FAD mouse model may be suitable for the study of specific aspects of AD-associated lipid dysregulation. Our data thus provides a frame of reference for lipids that can be targeted for therapeutic interrogation either through pharmacological or enzymatic manipulations, to improve learning and memory in the context of AD. In particular, PLD$_2$ isoform-specific inhibitors (56) may prove to be valuable therapeutic agents in AD and thus require further evaluation. Our study also provides further incentive to systemati-

cally analyze the various animal models of AD available in the biomedical community as well as to expand these types of profiling to other AD-vulnerable brain regions, so that a better understanding of AD-linked lipid dysfunction can be achieved.

REFERENCES

1. Foley, P. (2010) Lipids in Alzheimer disease. A century-old story. *Biochim. Biophys. Acta* **1801,** 750–753
2. Tanzi, R. E., and Bertram, L. (2005) Twenty years of the Alzheimer disease amyloid hypothesis. A genetic perspective. *Cell* **120,** 545–555
3. Bu, G. (2009) Apolipoprotein E and its receptors in Alzheimer disease. Pathways, pathogenesis, and therapy. *Nat. Rev. Neurosci.* **10,** 333–344
4. Hollingworth, P., Harold, D., Sims, R., Gerrish, A., Lambert, J. C., Carrasquillo, M. M., Abraham, R., Hamshere, M. L., Pahwa, J. S., Moskvina, V., Dowzell, K., Jones, N., Stretton, A., Thomas, C., Richards, A., Ivanov, D., Widdowson, C., Chapman, J., Lovestone, S., Powell, J., Proitsi, P., Lupton, M. K., Brayne, C., Rubinsztein, D. C., Gill, M., Lawlor, B., Lynch, A., Brown, K. S., Passmore, P. A., Craig, D., McGuinness, B., Todd, S., Holmes, C., Mann, D., Smith, A. D., Beaumont, H., Warden, D., Wilcock, G., Love, S., Kehoe, P. G., Hooper, N. M., Vardy, E. R., Hardy, J., Mead, S., Fox, N. C., Rossor, M., Collinge, J., Maier, W., Jessen, F., Ruther, E., Schurmann, B., Heun, R., Kolsch, H., van den Bussche, H., Heuser, I., Kornhuber, J., Wiltfang, J., Dichgans, M., Frolich, L., Hampel, H., Gallacher, J., Hull, M., Rujescu, D., Giegling, I., Goate, A. M., Kauwe, J. S., Cruchaga, C., Nowotny, P., Morris, J. C., Mayo, K., Sleegers, K., Bettens, K., Engelborghs, S., De Deyn, P. P., Van Broeckhoven, C., Livingston, G., Bass, N. J., Gurling, H., McQuillin, A., Gwilliam, R., Deloukas, P., Al-Chalabi, A., Shaw, C. E., Tsolaki, M., Singleton, A. B., Guerreiro, R., Muhleisen, T. W., Nothen, M. M., Moebus, S., Jockel, K. H., Klopp, N., Wichmann, H. E., Pankratz, V. S., Sando, S. B., Aasly, J. O., Barcikowska, M., Wszolek, Z. K., Dickson, D. W., Graff-Radford, N. R., Petersen, R. C., van Duijn, C. M., Breteler, M. M., Ikram, M. A., Destefano, A. L., Fitzpatrick, A. L., Lopez, O., Launer, L. J., Seshadri, S., Berr, C., Campion, D., Epelbaum, J., Dartigues, J. F., Tzourio, C., Alperovitch, A., Lathrop, M., Feulner, T. M., Friedrich, P., Riehle, C., Krawczak, M., Schreiber, S., Mayhaus, M., Nicolhaus, S., Wagenpfeil, S., Steinberg, S., Stefansson, H., Stefansson, K., Snaedal, J., Bjornsson, S., Jonsson, P. V., Chouraki, V., Genier-Boley, B., Hiltunen, M., Soininen, H., Combarros, O., Zelenika, D., Delepine, M., Bullido, M. J., Pasquier, F., Mateo, I., Frank-Garcia, A., Porcellini, E., Hanon, O., Coto, E., Alvarez, V., Bosco, P., Siciliano, G., Mancuso, M., Panza, F., Solfrizzi, V., Nacmias, B., Sorbi, S., Bossu, P., Piccardi, P., Arosio, B., Annoni, G., Seripa, D., Pilotto, A., Scarpini, E., Galimberti, D., Brice, A., Hannequin, D., Licastro, F., Jones, L., Holmans, P. A., Jonsson, T., Riemenschneider, M., Morgan, K., Younkin, S. G., Owen, M. J., O'Donovan, M., Amouyel, P., and Williams, J. (2011) *Nat. Genet.* **43,** 429–435
5. Naj, A. C., Jun, G., Beecham, G. W., Wang, L. S., Vardarajan, B. N., Buros, J., Gallins, P. J., Buxbaum, J. D., Jarvik, G. P., Crane, P. K., Larson, E. B., Bird, T. D., Boeve, B. F., Graff-Radford, N. R., De Jager, P. L., Evans, D., Schneider, J. A., Carrasquillo, M. M., Ertekin-Taner, N., Younkin, S. G., Cruchaga, C., Kauwe, J. S., Nowotny, P., Kramer, P., Hardy, J., Huentelman, M. J., Myers, A. J., Barmada, M. M., Demirci, F. Y., Baldwin, C. T., Green, R. C., Rogaeva, E., George-Hyslop, P. S., Arnold, S. E., Barber, R., Beach, T., Bigio, E. H., Bowen, J. D., Boxer, A., Burke, J. R., Cairns, N. J., Carlson, C. S., Carney, R. M., Carroll, S. L., Chui, H. C., Clark, D. G., Corneveaux, J., Cotman, C. W., Cummings, J. L., Decarli, C., Dekosky, S. T., Diaz-Arrastia, R., Dick, M., Dickson, D. W., Ellis, W. G., Faber, K. M., Fallon, K. B., Farlow, M. R., Ferris, S., Frosch, M. P., Galasko, D. R., Ganguli, M., Gearing, M., Geschwind, D. H., Ghetti, B., Gilbert, J. R., Gilman, S., Giordani, B.,

6. Di Paolo, G., and Kim, T. W. (2011) Linking lipids to Alzheimer disease. Cholesterol and beyond. *Nat. Rev. Neurosci.* **12,** 284–296
7. Grösgen, S., Grimm, M. O., Friess, P., and Hartmann, T. (2010) Role of amyloid β in lipid homeostasis. *Biochim. Biophys. Acta* **1801,** 966–974
8. Grimm, M. O., Grimm, H. S., Pätzold, A. J., Zinser, E. G., Halonen, R., Duering, M., Tschäpe, J. A., De Strooper, B., Müller, U., Shen, J., and Hartmann, T. (2005) Regulation of cholesterol and sphingomyelin metabolism by amyloid-β and presenilin. *Nat. Cell Biol.* **7,** 1118–1123
9. Sanchez-Mejia, R. O., Newman, J. W., Toh, S., Yu, G. Q., Zhou, Y., Halabisky, B., Cissé, M., Scearce-Levie, K., Cheng, I. H., Gan, L., Palop, J. J., Bonventre, J. V., and Mucke, L. (2008) Phospholipase A_2 reduction ameliorates cognitive deficits in a mouse model of Alzheimer disease. *Nat. Neurosci.* **11,** 1311–1318
10. Berman, D. E., Dall'Armi, C., Voronov, S. V., McIntire, L. B., Zhang, H., Moore, A. Z., Staniszewski, A., Arancio, O., Kim, T. W., and Di Paolo, G. (2008) Oligomeric amyloid-β peptide disrupts phosphatidylinositol 4,5-bisphosphate metabolism. *Nat. Neurosci.* **11,** 547–554
11. Oliveira, T. G., Chan, R. B., Tian, H., Laredo, M., Shui, G., Staniszewski, A., Zhang, H., Wang, L., Kim, T. W., Duff, K. E., Wenk, M. R., Arancio, O., and Di Paolo, G. (2010) Phospholipase D_2 ablation ameliorates Alzheimer disease-linked synaptic dysfunction and cognitive deficits. *J. Neurosci.* **30,** 16419–16428
12. Matsuzaki, K., Kato, K., and Yanagisawa, K. (2010) Aβ polymerization through interaction with membrane gangliosides. *Biochim. Biophys. Acta* **1801,** 868–877
13. Wenk, M. R. (2010) Lipidomics, new tools and applications. *Cell* **143,** 888–895
14. Han, X., Holtzman, D. M., and McKeel, D. W., Jr. (2001) Plasmalogen deficiency in early Alzheimer disease subjects and in animal models. Molecular characterization using electrospray ionization mass spectrometry. *J. Neurochem.* **77,** 1168–1180
15. Han, X., M. Holtzman, D., McKeel, D. W., Jr., Kelley, J., and Morris, J. C. (2002) Substantial sulfatide deficiency and ceramide elevation in very early Alzheimer disease. Potential role in disease pathogenesis. *J. Neurochem.* **82,** 809–818
16. Cutler, R. G., Kelly, J., Storie, K., Pedersen, W. A., Tammara, A., Hatanpaa, K., Troncoso, J. C., and Mattson, M. P. (2004) Involvement of oxidative stress-induced abnormalities in ceramide and cholesterol metabolism in brain aging and Alzheimer disease. *Proc. Natl. Acad. Sci. U.S.A.* **101,** 2070–2075
17. Ryan, S. D., Whitehead, S. N., Swayne, L. A., Moffat, T. C., Hou, W., Ethier, M., Bourgeois, A. J., Rashidian, J., Blanchard, A. P., Fraser, P. E., Park, D. S., Figeys, D., and Bennett, S. A. (2009) Amyloid-β42 signals Tau hyperphosphorylation and compromises neuronal viability by disrupting alkylacylglycerophosphocholine metabolism. *Proc. Natl. Acad. Sci. U.S.A.* **106,** 20936–20941
18. Raghu, P., Coessens, E., Manifava, M., Georgiev, P., Pettitt, T., Wood, E., Garcia-Murillas, I., Okkenhaug, H., Trivedi, D., Zhang, Q., Razzaq, A., Zaid, O., Wakelam, M., O'Kane, C. J., and Ktistakis, N. (2009) Rhabdomere biogenesis in *Drosophila* photoreceptors is acutely sensitive to phospha-

Glass, J. D., Growdon, J. H., Hamilton, R. L., Harrell, L. E., Head, E., Honig, L. S., Hulette, C. M., Hyman, B. T., Jicha, G. A., Jin, L. W., Johnson, N., Karlawish, J., Karydas, A., Kaye, J. A., Kim, R., Koo, E. H., Kowall, N. W., Lah, J. J., Levey, A. I., Lieberman, A. P., Lopez, O. L., Mack, W. J., Marson, D. C., Martiniuk, F., Mash, D. C., Masliah, E., McCormick, W. C., McCurry, S. M., McDavid, A. N., McKee, A. C., Mesulam, M., Miller, B. L., Miller, C. A., Miller, J. W., Parisi, J. E., Perl, D. P., Peskind, E., Petersen, R. C., Poon, W. W., Quinn, J. F., Rajbhandary, R. A., Raskind, M., Reisberg, B., Ringman, J. M., Roberson, E. D., Rosenberg, R. N., Sano, M., Schneider, L. S., Seeley, W., Shelanski, M. L., Slifer, M. A., Smith, C. D., Sonnen, J. A., Spina, S., Stern, R. A., Tanzi, R. E., Trojanowski, J. Q., Troncoso, J. C., Van Deerlin, V. M., Vinters, H. V., Vonsattel, J. P., Weintraub, S., Welsh-Bohmer, K. A., Williamson, J., Woltjer, R. L., Cantwell, L. B., Dombroski, B. A., Beekly, D., Lunetta, K. L., Martin, E. R., Kamboh, M. I., Saykin, A. J., Reiman, E. M., Bennett, D. A., Morris, J. C., Montine, T. J., Goate, A. M., Blacker, D., Tsuang, D. W., Hakonarson, H., Kukull, W. A., Foroud, T. M., Haines, J. L., Mayeux, R., Pericak-Vance, M. A., Farrer, L. A., and Schellenberg, G. D. (2011) *Nat. Genet.* **43,** 436–441

tidic acid levels. *J. Cell Biol.* **185,** 129–145

19. Wu, W., and Small, S. A. (2006) Imaging the earliest stages of Alzheimer disease. *Curr. Alzheimer Res.* **3,** 529–539

20. Gómez-Isla, T., Price, J. L., McKeel, D. W., Jr., Morris, J. C., Growdon, J. H., and Hyman, B. T. (1996) Profound loss of layer II entorhinal cortex neurons occurs in very mild Alzheimer disease. *J. Neurosci.* **16,** 4491–4500

21. Duff, K., Eckman, C., Zehr, C., Yu, X., Prada, C. M., Perez-tur, J., Hutton, M., Buee, L., Harigaya, Y., Yager, D., Morgan, D., Gordon, M. N., Holcomb, L., Refolo, L., Zenk, B., Hardy, J., and Younkin, S. (1996) Increased amyloid-β42(43) in brains of mice expressing mutant presenilin 1. *Nature* **383,** 710–713

22. Hsiao, K., Chapman, P., Nilsen, S., Eckman, C., Harigaya, Y., Younkin, S., Yang, F., and Cole, G. (1996) Correlative memory deficits, Aβ elevation, and amyloid plaques in transgenic mice. *Science* **274,** 99–102

23. Holcomb, L., Gordon, M. N., McGowan, E., Yu, X., Benkovic, S., Jantzen, P., Wright, K., Saad, I., Mueller, R., Morgan, D., Sanders, S., Zehr, C., O'Campo, K., Hardy, J., Prada, C. M., Eckman, C., Younkin, S., Hsiao, K., and Duff, K. (1998) Accelerated Alzheimer-type phenotype in transgenic mice carrying both mutant amyloid precursor protein and presenilin 1 transgenes. *Nat. Med.* **4,** 97–100

24. Gong, B., Cao, Z., Zheng, P., Vitolo, O. V., Liu, S., Staniszewski, A., Moolman, D., Zhang, H., Shelanski, M., and Arancio, O. (2006) Ubiquitin hydrolase Uch-L1 rescues β-amyloid-induced decreases in synaptic function and contextual memory. *Cell* **126,** 775–788

25. Cheng, D., Jenner, A. M., Shui, G., Cheong, W. F., Mitchell, T. W., Nealon, J. R., Kim, W. S., McCann, H., Wenk, M. R., Halliday, G. M., and Garner, B. (2011) Lipid pathway alterations in Parkinson disease primary visual cortex. *PLoS One* **6,** e17299

26. Chan, R., Uchil, P. D., Jin, J., Shui, G., Ott, D. E., Mothes, W., and Wenk, M. R. (2008) Retroviruses human immunodeficiency virus and murine leukemia virus are enriched in phosphoinositides. *J. Virol.* **82,** 11228–11238

27. Shui, G., Guan, X. L., Gopalakrishnan, P., Xue, Y., Goh, J. S., Yang, H., and Wenk, M. R. (2010) Characterization of substrate preference for Slc1p and Cst26p in *Saccharomyces cerevisiae* using lipidomic approaches and an LPAAT activity assay. *PLoS One* **5,** e11956

28. Shui, G., Guan, X. L., Low, C. P., Chua, G. H., Goh, J. S., Yang, H., and Wenk, M. R. (2010) Toward one step analysis of cellular lipidomes using liquid chromatography coupled with mass spectrometry. Application to *Saccharomyces cerevisiae* and *Schizosaccharomyces pombe* lipidomics. *Mol. Biosyst.* **6,** 1008–1017

29. Shui, G., Cheong, W. F., Jappar, I. A., Hoi, A., Xue, Y., Fernandis, A. Z., Tan, B. K., and Wenk, M. R. (2011) Derivatization-independent cholesterol analysis in crude lipid extracts by liquid chromatography/mass spectrometry. Applications to a rabbit model for atherosclerosis. *J. Chromatogr. A* **1218,** 4357–4365

30. Hodgkin, M. N., Pettitt, T. R., Martin, A., Michell, R. H., Pemberton, A. J., and Wakelam, M. J. (1998) Diacylglycerols and phosphatidates, which molecular species are intracellular messengers? *Trends Biochem. Sci.* **23,** 200–204

31. Schulze, H., Kolter, T., and Sandhoff, K. (2009) Principles of lysosomal membrane degradation. Cellular topology and biochemistry of lysosomal lipid degradation. *Biochim. Biophys. Acta* **1793,** 674–683

32. Bhattacharyya, R., and Kovacs, D. M. (2010) ACAT inhibition and amyloid β reduction. *Biochim. Biophys. Acta* **1801,** 960–965

33. Wang, G., Silva, J., Dasgupta, S., and Bieberich, E. (2008) Long-chain ceramide is elevated in presenilin 1 (PS1M146V) mouse brain and induces apoptosis in PS1 astrocytes. *Glia* **56,** 449–456

34. Sampaio, J. L., Gerl, M. J., Klose, C., Ejsing, C. S., Beug, H., Simons, K., and Shevchenko, A. (2011) Membrane lipidome of an epithelial cell line. *Proc. Natl. Acad. Sci. U.S.A.* **108,** 1903–1907

35. Andreyev, A. Y., Fahy, E., Guan, Z., Kelly, S., Li, X., McDonald, J. G., Milne, S., Myers, D., Park, H., Ryan, A., Thompson, B. M., Wang, E., Zhao, Y., Brown, H. A., Merrill, A. H., Raetz, C. R., Russell, D. W., Subramaniam, S., and Dennis, E. A. (2010) Subcellular organelle lipidomics in TLR-4-activated macrophages. *J. Lipid Res.* **51,** 2785–2797

36. Haass, C., and Selkoe, D. J. (2007) Soluble protein oligomers in neurodegeneration. Lessons from the Alzheimer amyloid β-peptide. *Nat. Rev. Mol. Cell Biol.* **8,** 101–112

37. Kim, K., Yang, J., and Kim, E. (2010) Diacylglycerol kinases in the regulation of dendritic spines. *J. Neurochem.* **112,** 577–587

38. Birnbaum, S. G., Yuan, P. X., Wang, M., Vijayraghavan, S., Bloom, A. K., Davis, D. J., Gobeske, K. T., Sweatt, J. D., Manji, H. K., and Arnsten, A. F. (2004) Protein kinase C overactivity impairs prefrontal cortical regulation of working memory. *Science* **306,** 882–884

39. Haughey, N. J., Bandaru, V. V., Bae, M., and Mattson, M. P. (2010) Roles for dysfunctional sphingolipid metabolism in Alzheimer disease neuropathogenesis. *Biochim. Biophys. Acta* **1801,** 878–886

40. Katsel, P., Li, C., and Haroutunian, V. (2007) Gene expression alterations in the sphingolipid metabolism pathways during progression of dementia and Alzheimer disease. A shift toward ceramide accumulation at the earliest recognizable stages of Alzheimer disease? *Neurochem. Res.* **32,** 845–856

41. Falguières, T., Luyet, P. P., and Gruenberg, J. (2009) Molecular assemblies and membrane domains in multivesicular endosome dynamics. *Exp. Cell Res.* **315,** 1567–1573

42. Cataldo, A. M., Mathews, P. M., Boiteau, A. B., Hassinger, L. C., Peterhoff, C. M., Jiang, Y., Mullaney, K., Neve, R. L., Gruenberg, J., and Nixon, R. A. (2008) Down syndrome fibroblast model of Alzheimer-related endosome pathology. Accelerated endocytosis promotes late endocytic defects. *Am. J. Pathol.* **173,** 370–384

43. Ginsberg, S. D., Alldred, M. J., Counts, S. E., Cataldo, A. M., Neve, R. L., Jiang, Y., Wuu, J., Chao, M. V., Mufson, E. J., Nixon, R. A., and Che, S. (2010) Microarray analysis of hippocampal CA1 neurons implicates early endosomal dysfunction during Alzheimer disease progression. *Biol. Psychiatry* **68,** 885–893

44. Small, S. A., and Gandy, S. (2006) Sorting through the cell biology of Alzheimer disease. Intracellular pathways to pathogenesis. *Neuron* **52,** 15–31

45. Nixon, R. A. (2007) Autophagy, amyloidogenesis, and Alzheimer disease. *J. Cell Sci.* **120,** 4081–4091

46. Hoetzl, S., Sprong, H., and van Meer, G. (2007) The way we view cellular (glyco)sphingolipids. *J. Neurochem.* **103,** Suppl. 1, 3–13

47. Kobayashi, T., Stang, E., Fang, K. S., de Moerloose, P., Parton, R. G., and Gruenberg, J. (1998) A lipid associated with the antiphospholipid syndrome regulates endosome structure and function. *Nature* **392,** 193–197

48. Tamboli, I. Y., Hampel, H., Tien, N. T., Tolksdorf, K., Breiden, B., Mathews, P. M., Saftig, P., Sandhoff, K., and Walter, J. (2011) Sphingolipid storage affects autophagic metabolism of the amyloid precursor protein and promotes Aβ generation. *J. Neurosci.* **31,** 1837–1849

49. Simons, K., and Gruenberg, J. (2000) Jamming the endosomal system. Lipid rafts and lysosomal storage diseases. *Trends Cell Biol.* **10,** 459–462

50. Dall'Armi, C., Hurtado-Lorenzo, A., Tian, H., Morel, E., Nezu, A., Chan, R. B., Yu, W. H., Robinson, K. S., Yeku, O., Small, S. A., Duff, K., Frohman, M. A., Wenk, M. R., Yamamoto, A., and Di Paolo, G. (2010) The phospholipase D1 pathway modulates macroautophagy. *Nat. Commun.* **1,** 142

51. Spector, A. A., and Yorek, M. A. (1985) Membrane lipid composition and cellular function. *J. Lipid Res.* **26,** 1015–1035

52. Osenkowski, P., Ye, W., Wang, R., Wolfe, M. S., and Selkoe, D. J. (2008) Direct and potent regulation of γ-secretase by its lipid microenvironment. *J. Biol. Chem.* **283,** 22529–22540

53. Mateos, M. V., Salvador, G. A., and Giusto, N. M. (2010) Selective localization of phosphatidylcholine-derived signaling in detergent-resistant membranes from synaptic endings. *Biochim. Biophys. Acta* **1798,** 624–636

54. Martín, V., Fabelo, N., Santpere, G., Puig, B., Marín, R., Ferrer, I., and Díaz, M. (2010) Lipid alterations in lipid rafts from Alzheimer disease human brain cortex. *J. Alzheimers Dis.* **19,** 489–502

55. Wassall, S. R., and Stillwell, W. (2009) Polyunsaturated fatty acid-cholesterol interactions. Domain formation in membranes. *Biochim. Biophys. Acta* **1788,** 24–32

56. Lavieri, R. R., Scott, S. A., Selvy, P. E., Kim, K., Jadhav, S., Morrison, R. D., Daniels, J. S., Brown, H. A., and Lindsley, C. W. (2010) Design, synthesis, and biological evaluation of halogenated *N*-(2-(4-oxo-1-phenyl-1,3,8-triazaspiro[4.5]decan-8-yl)ethyl)benzamides. Discovery of an isoform-selective small molecule phospholipase D$_2$ inhibitor. *J. Med. Chem.* **53,** 6706–6719